# Tailoring the morphology and properties of starch aerogels and cryogels via starch source and process parameter

Fangxin Zou, Tatiana Budtova

*Submitted to Carbohydrate Polymers 28 August 2020*

*Revised 12 October 2020*

# Tailoring the morphology and properties of starch aerogels and cryogels via starch source and process parameter

Fangxin Zou, Tatiana Budtova*

Center for Materials Forming - CEMEF, MINES ParisTech, PSL Research University, UMR CNRS 7635, CS 10207, 06904 Sophia Antipolis, France

* Corresponding author:

Tatiana Budtova, Tatiana.Budtova@mines-paristech.fr

## Abstract

Porous starch materials with various morphology and properties were made via starch dissolution, retrogradation and drying either with supercritical $CO_2$ ("aerogels") or lyophilisation ("cryogels"). Their properties were correlated with the rheological response of retrograded starch gels and crystallinity of aerogels and cryogels. All starch cryogels possess very low density (0.07 – 0.16 g/cm$^3$), very large macropores and low specific surface area (around 3 – 13 m$^2$/g). Their morphology is mainly the replica of sublimated ice crystals. The properties of starch aerogels strongly depend on starch source: the lowest density (around 0.1 g/cm$^3$) and highest specific surface area (170 – 250 m$^2$/g) was recorded for pea starch aerogels and the highest density (0.3 – 0.6 g/cm$^3$) and lowest specific surface area (7 – 90 m$^2$/g) for waxy maize starch aerogels. The morphology and properties of starch aerogels are interpreted by amylose and amylopectin evolution during retrogradation.



Keywords: supercritical drying, freeze-drying, morphology; density; specific surface area

## 1. Introduction

Starch is one of the most abundant polysaccharides used in multiple applications: in food and non-food (biodegradable films and foams for packaging, as additive in paper and textile) and also as a source of low molecular weight chemicals. Porous starch makes a special family of lightweight materials in which pore sizes, porosity and cellular morphology depend on the processing method: for example, voids are formed during extrusion of starch/water at high temperatures, baking a starch paste followed by water evaporation, microwave heating which generates steam bubbles, freeze-drying/sublimation of ice crystals and supercritical fluid extrusion. Rather recently, supercritical fluid extraction technique, used to make aerogels, has also been applied to starch.

Aerogels are nanostructured lightweight mesoporous/small macropores materials with high specific surface area (of several hundreds of $m^2/g$); the latter distinguishes them from foams which usually are lightweight but with very large macropores and thus low surface area. The very first aerogels were reported by Kistler in 1931 (Kistler, 1931); inorganic aerogels were then developed in the 70s-80s of the past century followed by aerogels based on synthetic polymers (Pierre, 2011). Aerogels are versatile materials: they can be used for water-oil separation (Sai et al., 2015; Zou, Peng, Fu, Zhang, & Li, 2015), thermal insulation (Groult & Budtova, 2018a; Zou et al., 2016), drug delivery (Mehling, Smirnova, Guenther, & Neubert, 2009; Ulker & Erkey, 2014) and electro-chemical/energy storage (Hamedi et al., 2013; Rooke et al., 2011) applications. In the past two decades, a variety of so-called bio-aerogels made from polysaccharides such as cellulose (Lavoine & Bergström, 2017; Budtova, 2019), pectin (Zhao, Chen, & Chen, 2017; Groult & Budtova, 2018b), starch (García-González, Uy, Alnaief, & Smirnova, 2012; Zhu, 2019), and alginate (Mallepally, Bernard, Marin, Ward, & McHugh, 2013; Robitzer, David, Rochas, Renzo, & Quignard, 2008) gained widespread attention in the view of the need of sustainable and biodegradable materials on the one hand, and their potential use in biomedical applications on the other hand.

As most of bio-aerogels (except those based on nanocellulose), starch aerogels are made via dissolution-gelation (retrogradation for starch)-solvent exchange-drying with supercritical carbon dioxide. Starch aerogels were shown to be promising matrices for drug release (García-González et al., 2012; Mehling et al., 2009) and also for thermal insulation (Druel, Bardl, Vorwerg, & Budtova, 2017). It was reported that higher starch concentration, higher aerogel density (García-González & Smirnova, 2013; Ubeyitogullari & Ciftci, 2016), as expected. It seems that higher amylose content

leads to higher specific surface area, for example, 200 – 250 $m^2/g$ for pea and high amylose corn (Druel et al., 2017; García-González et al., 2013) vs 20 – 80 $m^2/g$ for potato (Druel et al., 2017) and wheat starches (Ubeyitogullari et al., 2016). However, low specific surface area, 90 $m^2/g$, was reported for high amylose starch Eurylon 7 (Mehling et al., 2009), most probably because of incomplete starch dissolution. There are still several open questions such as the influence of the starch type and retrogradation time on aerogel structure and properties.

It should be noted that the first mention of using drying with supercritical $CO_2$ for making starch aerogels was made by Glenn *et al,* and the materials were called "microcellular foams" (Glenn & Irving, 1995). This seminal work compared the structure and properties of freeze-dried and supercritically dried unmodified wheat starch, regular corn and high amylose corn starches. However, starch granule remnants were present in the dried samples and samples' specific surface area was not measured; low-resolution scanning electron microscope (SEM) did not allow the analysis of microstructure below one micron.

As mentioned above, another way of making porous starch materials avoiding pores' collapse during drying is freeze-drying. Freeze-dried starch can be used in multiple applications, mainly in food and also in biomedical area (for example, in tissue engineering). Numerous studies have been performed on freeze-dried starches, either on starch granules (B. Zhang et al., 2014), or on starch solutions alone or mixed with other natural components (Nakamatsu, Torres, Troncoso, Min-Lin, & Boccaccini, 2006; Svagan, Samir, & Berglund, 2008), or on starch emulsions (Silva, Azevedo, Cunha, Hubinger, & Meireles, 2016; Spada, Norena, Marczak, & Tessaro, 2012). In food applications, freeze-drying is considered as a way of granules' preservation, and the influence of drying method (oven drying from water or ethanol, freeze-drying, microwave drying, etc) on starch gelatinization and digestibility was investigated (Glenn et al., 2008; B. Zhang et al., 2014). In materials science freeze-drying is used to shape the pores of starch solution (usually strong retrogradation is avoided) upon removing water (Nakamatsu et al., 2006; Svagan et al., 2008). When using starch for encapsulation, freeze-drying allows obtaining powders and is often compared with spray drying (Silva et al., 2016; Spada et al., 2012).

To the best of our knowledge, there is no study, except the one of Glenn *et al* (Glenn et al, 1995), on the comparison of the structure and properties of freeze-dried and supercritical dried starches made from the same starting gels. How does the way of drying and starch type (i.e.

amylose/amylopectin ratio) influence starch morphology and properties? It is well documented that retrogradation kinetics depends on amylose/amylopectin ratio: gelation is faster in high-amylose starches as amylose undergoes rapid recrystallization forming semi-crystalline clusters. What is the impact, if any, of retrogradation time on freeze-dried and supercritically dried starch gels? The answers to these questions will help tuning starch morphology and properties for the desired applications.

The goal of this work is to understand the influence of starch type (amylose content) and processing conditions (way of drying, starch concentration, retrogradation time) on the morphology and properties of porous starches starting from the same precursor. For simplicity, we will use "aerogels" for samples dried with supercritical $CO_2$, and "cryogels" for freeze-dried samples. We correlate the morphology and properties of porous starches with their crystallinity and gel strength, and we suggest using "aerogel approach" as a way to follow starch gel structure evolution upon retrogradation and as a function of amylose content.

## 2. Experimental

### 2.1 Materials

Three types of starches were kindly provided by Roquette, France: waxy maize, potato and pea with amylose content around 1%, 18-21%, and 33-36%, respectively. Absolute ethanol (>99%) was purchased from Fisher Scientific. Distillated water was used. All chemicals were used without any further purification.

### 2.2 Preparation of starch solutions and gels

Starch needs to be dissolved as well as possible in order to avoid the presence of non-dissolved granules and their remnants. The residual granules and their remnants are non-porous and may decrease the specific surface areas of aerogels in a similar manner as non-dissolved cellulose fibers decreased specific surface area in cellulose aerogels (Korhonen & Budtova, 2020).

Different methods were adapted to dissolve the three types of starches because of their different solubility in water. Optical microscopy (LEICA DM4500P, Leica Microsystems) was used for the screening of the influence of the dissolution conditions on the presence of granules' remnants (Table S1 in the Supporting Information). The final conditions selected for each starch type were when no non-dissolved fragments were seen in optical micrographs. For example, no non-dissolved granules

were detected when stirring potato starch dispersed in water at 1000 rpm at 95 °C for 2 h, but 3 h were needed to dissolve waxy maize starch in the same conditions (Table S1). To dissolve pea starch two steps method (Druel et al., 2017) was used: first, pea starch-water was heated to 95 °C under stirring at 1000 rpm for 1 h; then this mixture was placed in the autoclave (452HC, Parr instrument), heated during 50 min up to 130 °C and kept at 130-140 °C for another 20 min under stirring at 250 rpm.

Starch solutions of various concentrations, from 5 to 11 wt% (in dry weight), were prepared as described above for each type of starch. Hot starch solutions were centrifuged, if needed, for 3 min under 8000 rpm to remove bubbles and poured into plastic molds. After cooling down to room temperature, all samples were stored at 4 °C for retrogradation. The retrogradation time for potato and pea starch was from 1 to 4 days and for waxy maize from 15 to 45 days. Long retrogradation times of waxy maize starch solutions were needed as in non-gelled state solution viscosity was too low not allowing making homogeneous aerogels and cryogels. In the following, starch gels are named as "starch type-Xwt%-Nday-gel", where X is starch concentration in solution and N is retrogradation time.

2.3 Preparation of starch aerogels and cryogels

Starch aerogels were prepared according to the following steps: dissolution-retrogradation-solvent exchange-supercritical $CO_2$ drying. Before drying, water was replaced by ethanol through solvent exchange as water is not miscible with supercritical $CO_2$. The solvent exchange was performed by gradual increase of ethanol in ethanol/water mixtures: first, the gels were soaked in ethanol/water 50/50 (v/v) for 0.5 day, then in ethanol/water 75/25 (v/v) for another 0.5 day, and finally in pure ethanol for 3 days during which fresh ethanol was exchanged twice a day.

Supercritical $CO_2$ drying was performed as follows. First, ethanol in the gel was slowly drained by gaseous $CO_2$ while the system was pressurized at 50 bar and 37 °C. Then, the temperature was set at 37 °C, and the pressure was increased to 80 bar above $CO_2$ critical point. After that, a dynamic washing step was performed at 80 bar and 37 °C with an output of 5 kg/h of $CO_2$ for 1 h to remove the residual ethanol from the gel. It was followed by a static mode for 1-2 h under the same temperature and pressure and dynamic washing step again for 2 h. Finally, the system was kept at 37 °C and slowly depressurized to ambient conditions with pressure decrease speed 5 bar/h. Slow depressurization was used to prevent sample strong shrinkage. The autoclave was cooled down to

156 room temperature before being opened. Starch aerogels are named as “starch type-Xwt%-Nday-
157 aerogel” where X and N are the same as for starch gels.

158 Starch cryogels were prepared from gels using freeze drying. The gels were unidirectionally frozen
159 by placing starch gel on a metal plate which was immersed in liquid nitrogen for 20 min, and then
160 freeze-dried for 72 h at -82 °C and pressure below 2 mTorr by using the Lyophilisateur Cryotec
161 COSMOS-80 (Cryotec). In the following, the starch cryogels are named as “starch type-Xwt%-Nday-
162 cryogel” where X and N are the same as for starch gels.

163 2.4 Characterization

164 2.4.1 Rheology

165 The rheological properties of starch gels were probed using Gemini 150 rheometer (Bohlin
166 Instruments) with parallel plate geometry (40 mm diameter) and gap 1000 µm. A hot starch solution
167 was put on the lower plate, kept for 1.5 min, gap closed and the whole kept for another 3 min.
168 Temperature was then set at 4 °C for different retrogradation times varying from 1 to 4 days before
169 starting the oscillation. Strain response of elastic (G’) and viscous (G”) moduli was tested at 4 °C to
170 determine the mechanical response of starch gels to shear strain in the range 0.1% - 1000% at
171 frequency 1 Hz. The diameter of plates was varied to test the potential slippage; no influence of plates’
172 geometry on G’ and G” values was recorded, within the experimental errors, indicating the absence of
173 slippage.

174 2.4.2 Linear shrinkage

175 The total linear shrinkage of the samples due to the solvent exchange and drying was calculated
176 according to the following equation with at least three measurements per formulation (Himmel, Gerber,
177 Biirger, Holzhfiter, & Olbertz, 1995; Saliger, Heinrich, Gleissner, & Fricke, 1995):

178 $$\text{Linear shrinkage} = \frac{D_b - D_a}{D_b} \times 100\% \quad (1)$$

179 where $D_b$ and $D_a$ are the diameters of sample before solvent exchange and after drying, respectively.

180 2.4.3 Bulk density and porosity

181 Bulk density of starch aerogels and cryogels was determined by Geopyc 1360 (Micromeritics)
182 powder densitometer with Dryflo as the powder, with at least five measurements per formulation. The
183 diameter of the test chamber was 19.1 mm, and the force was 25 N.

184 The porosity (%) of each sample was calculated as follows:

185 $$\text{Porosity} = \frac{\rho_s - \rho_b}{\rho_s} \times 100\% \quad (2)$$

where $\rho_b$ and $\rho_s$ refer to the bulk and skeletal densities, respectively, with $\rho_s$ =1.45 g/cm$^3$ (García-González et al., 2013).

2.4.4 Specific surface area

Specific surface area ($S_{BET}$) of starch aerogels and cryogels was calculated using nitrogen adsorption method with ASAP 2020 specific surface area and porosity analyzer (Micromeritics Instrument Corporation). Prior to the measurement, all samples were degassed at 70 °C for 10 h. The maximal standard deviation was 12 m$^2$/g.

2.4.5 Scanning electron microscope

The morphology of starch samples was characterized by Scanning Electron Microscope (SEM) Supra40 Zeiss SEM FEG (Fields Emission Gun) (ZEISS) with an accelerating voltage of 3 kV and diaphragm 10 µm. Before the measurements, a roughly 7 nm thin layer of platinum was sputtered onto the sample's surface with Q150T coater (Quorum).

2.4.6 X-ray diffraction analysis

X-ray diffraction (XRD) analysis (in reflection mode) was performed on diffractometer "XPERT-PRO" (PANalytical) with Cu $K_\alpha$ radiation at wavelength of 1.5406 Å. The samples were grinded into powder and scanned in 2θ range from 5° to 50°. The relative crystallinity was calculated by the following equation:

$$\text{Relative crystallinity} = \frac{A_c}{A_c + A_a} \times 100\% \quad (3)$$

where $A_c$ and $A_a$ are the integrated areas of crystalline and amorphous regions, respectively, over the 2θ range from 5° to 28°. $A_c$ and $A_a$ were calculated using the method of Komiya and Nara (Komiya & Nara, 1986; Cheetham & Tao, 1998). Komiya & Nara showed that XRD in symmetrical reflection and symmetrical transmission modes provide almost the same values of the relative crystallinity (Komiya & Nara, 1986).

## 3. Results

3.1 X-ray diffraction

An example of the relative crystallinity of starch aerogels and cryogels as a function of retrogradation time is shown in Figure 1a for pea starch aerogels and cryogels, and in Figures S1b and S1c (Supporting Information) for other starches. The examples of the diffraction profiles are shown in Figure S1a of the Supporting Information; sharp peaks on XRD profiles of the initial starches

become much weaker and broader after dissolution-retrogradation, as expected (Shi & Gao, 2016; Soest, Tournois, Wit, & Vliegenthart, 1995; Cheetham & Tao, 1998; Zhang, Hou, Liu, Wang, & Dong, 2019). As a consequence, the crystallinity of the initial starch significantly decreases after the dissolution-retrogradation-drying for all starches studied (Figure 1b). The decrease of the crystallinity of starch in wheat starch aerogels as compared to the initial starch have been reported previously (Ubeyitogullari et al., 2016). Figure 1a shows that drying method does not influence the crystallinity of pea starch; the same result was observed for potato and waxy maize starch (Figure S1b and S1c, respectively), and also for cellulose aerogels and cryogels (Buchtova, Pradille, Bouvard, & Budtova, 2019). The crystallinity of aerogels slightly increases with the increase of retrogradation time for all starches (Figure 1b), and it is the highest for pea starch which contains the highest amount of amylose. The latter is known for much faster crystallization than amylopectin (Ma, Ma, Zhou, Li, & Hu, 2019; Shi et al., 2016).

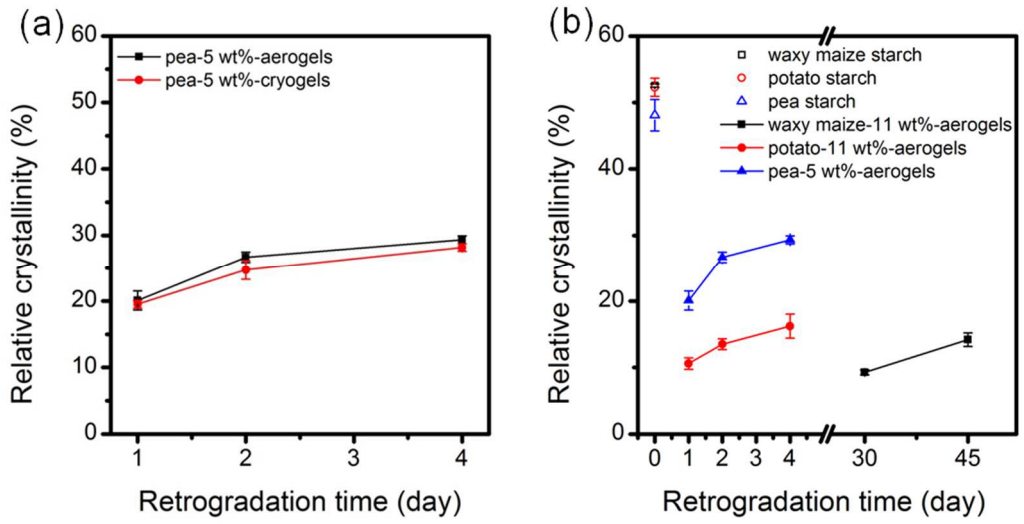


**Figure 1.** Relative crystallinity as a function of retrogradation time for (a) pea starch aerogel and cryogel and (b) aerogels from all three types and initial starches (retrogradation time 0). Lines are given to guide the eye. When standard deviation is not visible, it is smaller than the size of the symbol.

3.2 Rheological properties of starch gels

The examples of the dependences of storage and loss moduli on shear strain for potato and pea starch gels are presented in Figure 2. For all gels the elastic behavior dominates the viscous one, as expected, as potato and pea starch solutions are retrograded. For potato gels both moduli remain

constant within the wide strain interval: at high strains, around 100%, these gels first show strain hardening and then break (Figure 2a). No strain hardening was observed for pea starch gels (Figure 2b).

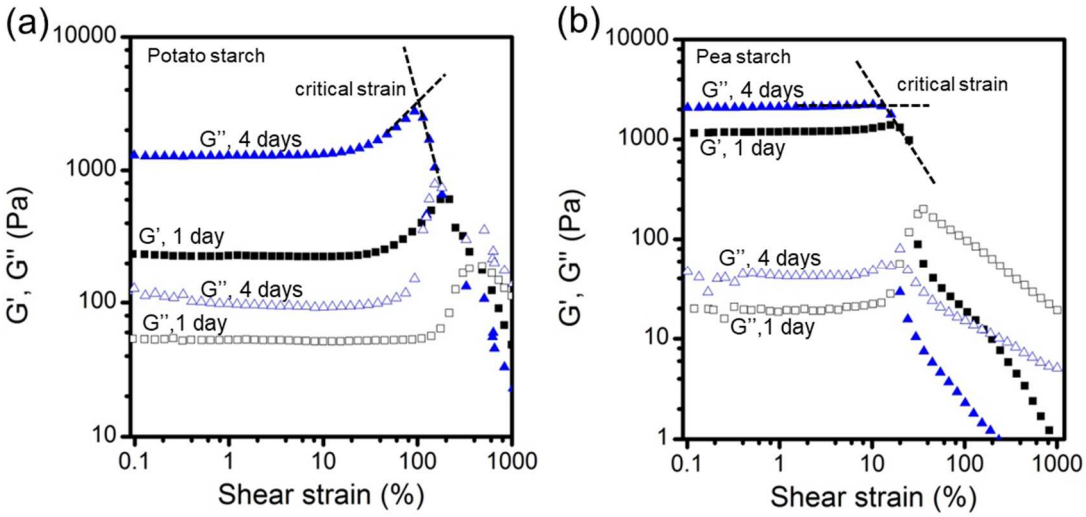


**Figure 2.** Representative dependences of storage modulus (G', filled points) and loss modulus (G'', open points) as a function of shear strain at different retrogradation times for (a) potato-11wt%-gels and (b) pea-5wt%-gels. Dashed lines are showing the determination of the critical strain.

The storage modulus in the linear region, $G_0'$, is plotted vs. retrogradation time in Figure 3a for all starch gels. Higher starch concentration, denser the network and thus higher $G_0'$, as expected. For example, for potato starch gels retrograded for 4 days the $G_0'$ value increases from 141 Pa to 1290 Pa for starch concentration varying from 8 wt% to 11 wt% (Figure 3a). The increase of retrogradation time also leads to $G_0'$ increase for both types of starches. Interestingly, $G_0'$ of 5 wt% pea starch gels is higher than that of potato starch gels of even higher concentrations, 8 wt% and 11 wt% (Figure 3a). The reason is that pea starch contains higher amount of amylose which is known to retrograde quicker than amylopectin and forms more crystalline regions (Putaux, Bule, & Chanzy, 2000) as reflected by higher relative crystallinity (Figure 1b).

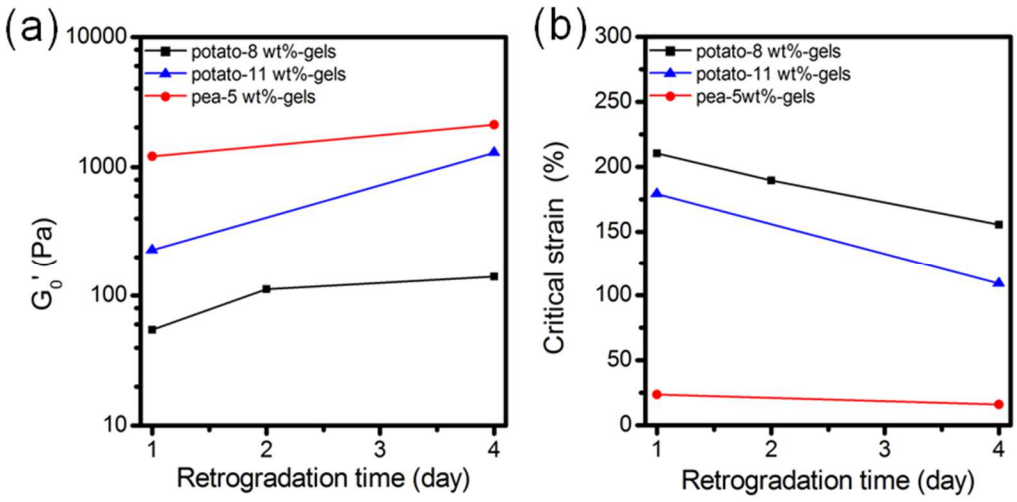


**Figure 3.** Storage moduli $G_0'$ (a) and critical strain (b) of pea and potato starch gels as a function of retrogradation time. Lines are given to guide the eye

Critical strain is determined as the value at which gel starts to break, see details in Figure 2a and b. The critical strain is plotted vs. retrogradation time in Figure 3b for the studied starch gels. Opposite to the storage modulus $G_0'$, critical strain decreases with increasing retrogradation time and starch concentration indicating that gels become more brittle. The most brittle are pea starch gels. Overall, the mechanical properties of starch gels correlate well with relative crystallinity data: the higher amylose content and longer retrogradation time, the higher is relative crystallinity and the stronger and more brittle are starch gels.

3.3 Starch aerogels: morphology and properties

The examples of the inner morphology of starch aerogels is shown in Figure 4 (a-h for lower magnification and i-k for higher magnification) for starches of different concentrations and retrograded at different times. More examples are presented in Figure S2 and S3 of the Supporting Information. Starch type has a significant influence on aerogel morphology: higher amylose content (pea>potato>waxy maize), finer and more ramified is aerogel structure. Waxy maize starch aerogels consist of rather smooth beads assembled together. Waxy maize starch solutions are retrograding very slowly as they are based on amylopectin and even at long retrogradation times the gels are very weak. We hypothesize that when these weak gels are placed in a non-solvent (ethanol), phase separation occurs according to spinodal decomposition mechanism, which is also the case when

cellulose is coagulated in a non-solvent directly from solutions resulting in aerogels with morphology represented by assembled together “hairy” beads (Buchtová & Budtova, 2016; Pircher et al., 2016; Sescousse, Gavillon, & Budtova, 2011). Interestingly, the surface of the beads in the internal structure of waxy maize aerogels is smooth but it seems that inside they are porous (Figure 4k). However, this porosity is observable in the fracture zones only where aerogel was broken for SEM observations. Potato starch aerogels contain a “mixture” of smooth beads and fine network while pea starch aerogels’ morphology is represented by a fine network. The strength of a starch gel before the sample is placed in a non-solvent plays an important role in structure formation: stronger is the gel (case of pea starch), better it is keeping the ramified network structure. In weak gels (case of waxy maize starch) amylopectin chains have more freedom to move, they form polymer rich phases upon the addition of non-solvent and undergo phase separation driven by spinodal decomposition.

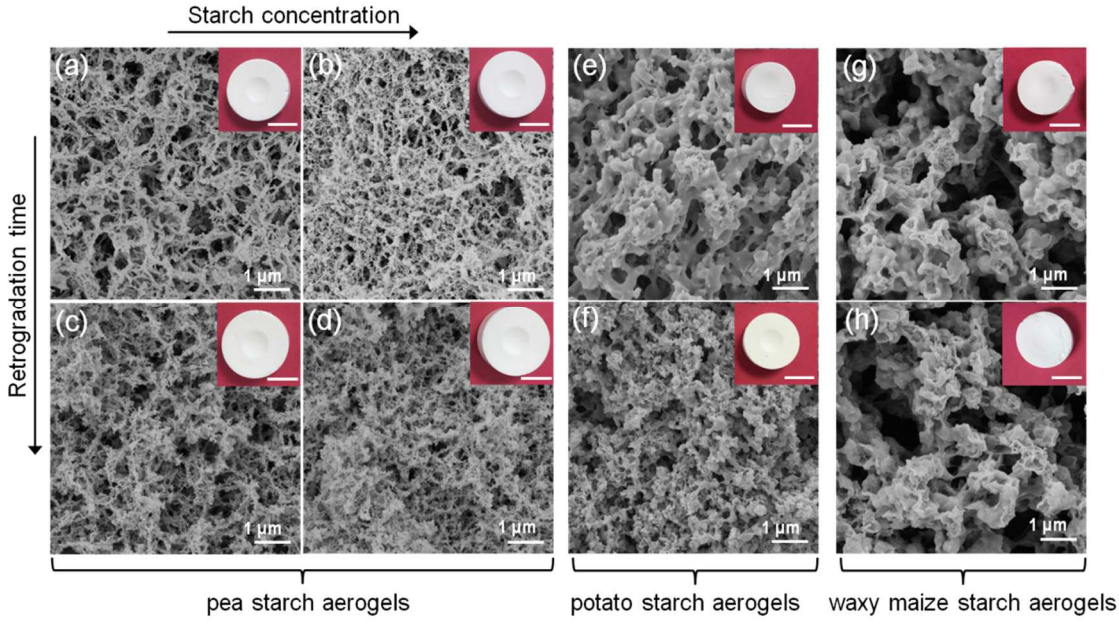


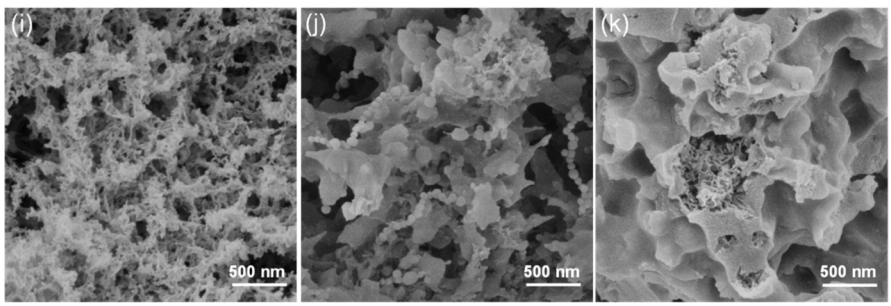

**Figure 4.** SEM images of aerogels internal morphology, insets are the digital photos of aerogel samples: (a) pea-5wt%-1day-aerogel, (b) pea-8wt%-1day-aerogel, (c) pea-5wt%-4day-aerogel, (d) pea-8wt%-4day-aerogel, (e) potato-11wt%-1day-aerogel, (f) potato-11wt%-4day-aerogel, (g) waxy maize-11wt%-30day-aerogel, (h) waxy maize-11wt%-45day-aerogel, (i) pea-8wt%-4day-aerogel, (j) potato-8wt%-4day-aerogel and (k) waxy maize-8wt%-15day-aerogel. The scale bars for photos of aerogels are 1 cm.

Higher starch concentration leads to denser network morphology (see Figure 4 for pea starch aerogels), the same was observed for other bio-aerogels (Buchtová et al, 2016; Groult et al, 2018b). Longer retrogradation times induce more ramified structure for amylose-containing starches (Figure 4).

Aerogel density and specific surface area are summarized in Fig. 5, and linear shrinkage (eq.1) and porosity (eq. 2) in Figure S4. Pea starch aerogels possess the lowest shrinkage, lowest density and highest porosity at all concentrations and retrogradation times: higher amylose content in starch leads to quicker retrogradation, highest relative crystallinity (Figure 1) and strongest gels (Figure 3a), helping to “resist” solvent exchange and drying. Higher starch concentration, lower shrinkage, as higher polymer concentration also leads to stronger gels. The same phenomenon was observed for cellulose and pectin aerogels (Buchtová et al, 2016; Groult et al, 2018b). Despite lower shrinkage with the increase of starch concentration, density increases (García-González et al., 2013; Ubeyitogullari et al., 2016) and porosity decreases, which shows that added matter “dominates” small gain in volume (Figure 5a and S4b). A strong influence of retrogradation time on shrinkage (Figure S4a), density (Figure 5a) and porosity (Figure S4b) is recorded for waxy maize aerogels as even retrograded for a long time (15 days) the gels are very weak and contract under solvent exchange and drying, as in the case of non-gelled pectin solutions (Groult et al., 2018b).

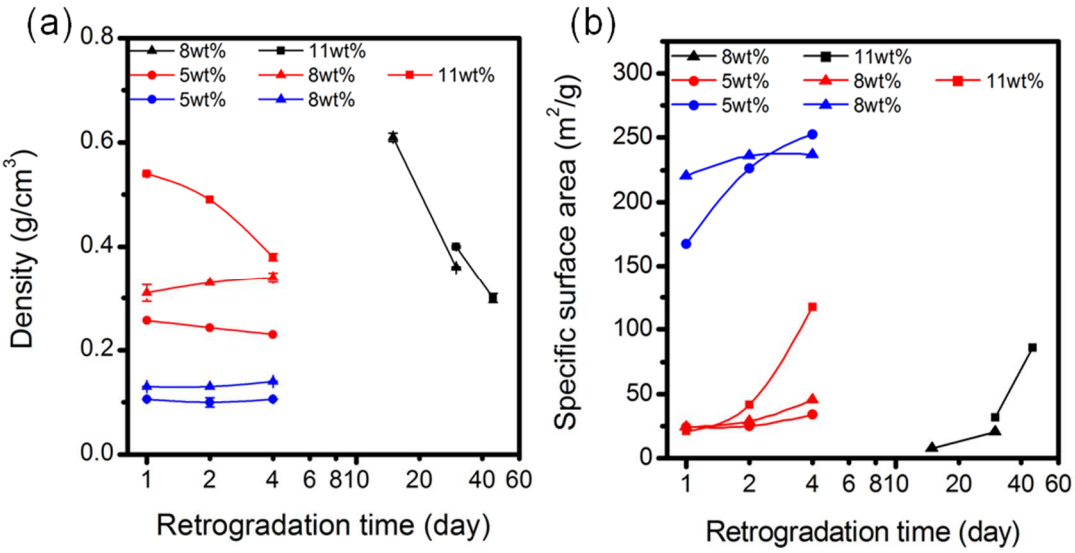


**Figure 5.** Density (a) and specific surface area (b) of starch aerogels from different starch sources and concentrations as a function of retrogradation time. Black, red, and blue data points correspond to waxy maize, potato and pea starch aerogels, respectively. Lines are given to guide the eye. If standard deviations for density values are not visible, they are within the dimension of the symbol.

Pea starch aerogels show the highest specific surface area among all aerogels studied, from around 160 - 250 $m^2/g$ vs 8 - 120 $m^2/g$ for potato and waxy maize aerogels (Figure 5b). Fine and ramified morphology of pea starch aerogels is the reason of higher specific surface are, see Figure 4. Specific surface area increases with the increase of starch concentration and of retrogradation time (Figure 5b). For cellulose aerogels it was suggested that higher polymer concentration leads to the ‘‘division’’ of pores into smaller ones thus increasing specific surface area (Buchtová et al., 2016); the same can also be assumed for starch aerogels. Network ramification with retrogradation time shown by SEM (Figure 4) confirms the increase of specific surface area.

### 3.4 Starch cryogels: morphology and properties

The morphology of starch cryogels is shown in Figure 6, more SEM images for potato and waxy maize starch cryogels can be found in Figures S5 and S6, respectively. All cryogels have very large macropores which are the replica of ice crystals that grew under freezing and “pushed aside” pore walls of starch gel. The pore sizes, as seen from SEM images, are smaller (especially for pea cryogels) than those reported in literature for the cases of freeze-dried amylopectin (7 days retrogradation) or

non-retrograded potato and corn starch solutions (Nakamatsu et al., 2006; Svagan et al., 2008). As all our samples were prepared in the same freezing and lyophilization conditions, it is the intrinsic properties of the starch that influence cryogel morphology. Stronger are the gels, better they "resist" to the growth of ice crystals. The pores in the retrograded pea starch aerogels do not show any preferential orientation despite unidirectional freezing; potato starch gels are weaker than pea starch and pores become oriented, and the weakest gels are those based on waxy maize starch and pores are strongly oriented in the direction of the growth of ice crystals as in the case of nanocellulose (Chau et al., 2016). Waxy maize starch is thus suitable for ice templating method. Potato and waxy maize starch cryogels have smooth pore walls, as in the case of amylopectin freeze-dried starch (Svagan et al., 2008), while those of pea starch are thinner and the network is more ramified. Pores with smooth walls and no preferential orientation were observed for cellulose cryogels made via unidirectional or isotropic freeze drying (Buchtová et al., 2016). In that case the structure of the network of cellulose coagulated in water resisted the unidirectional growth of ice crystals but resulted in smooth and thick pore walls and pore's size smaller than in starch cryogels.

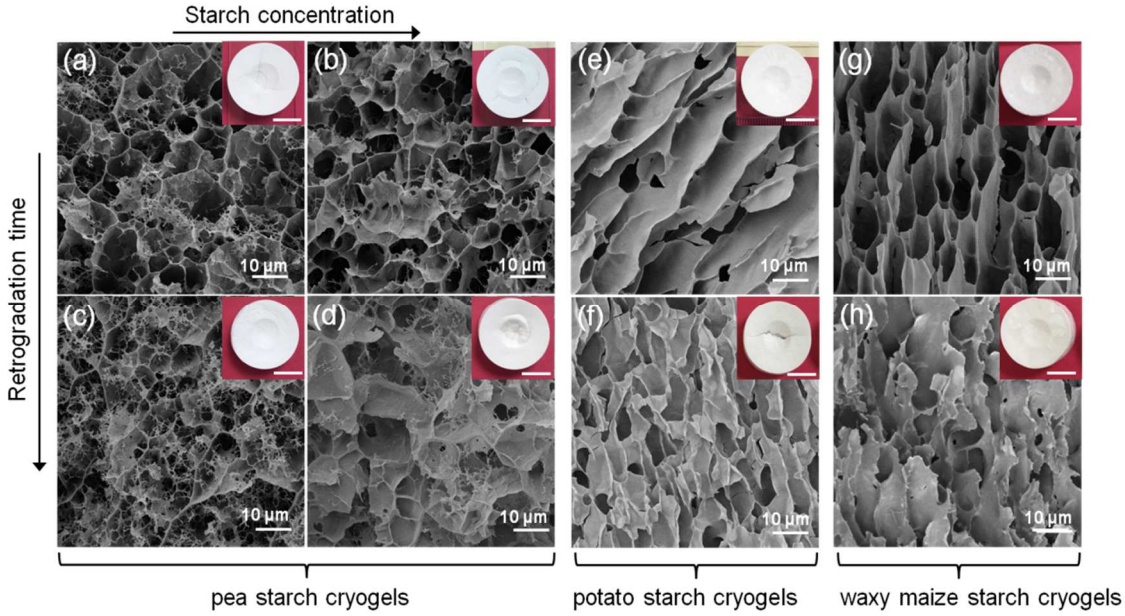


**Figure 6.** SEM images of cryogels' internal morphology, the insets show the digital photos of cryogels: (a) pea-5wt%-1day-cryogel, (b) pea-8wt%-1day-cryogel, (c) pea-5wt%-4day-cryogel, (d) pea-8wt%-4day-cryogel, (e) potato-8wt%-1day-cryogel, (f) potato-8wt%-4day-cryogel, (g) waxy mazie-8wt%-30day-cryogel and (h) waxy mazie-8wt%-45day-cryogel. The scale bars for photos of cryogels are 1 cm.

The increase of starch concentration seems to slightly decrease pore sizes of cryogels (Figures 6, S5 and S6), however, it is retrogradation time which impacts starch cryogel morphology: the longer retrogradation, the smaller the pores for all types of starches used in this work. The same was observed for all starch aerogels and is the sign of starch network ramification during retrogradation.

The density, porosity and specific surface area of all starch cryogels are summarized in Figure 7 and S4c as a function of retrogradation time. Practically no shrinkage was observed as no solvent/non-solvent exchange was performed for the preparation of cryogels. All cryogels have very low density, lower than that of aerogels, 0.07 - 0.16 vs 0.1 - 0.6 g/cm$^3$; a similar trend was reported for cellulose aerogels and cryogels (Buchtová et al., 2016). Higher starch concentration led to higher cryogel density and lower porosity, as expected, and no influence of retrogradation time was observed (Figure 7a).

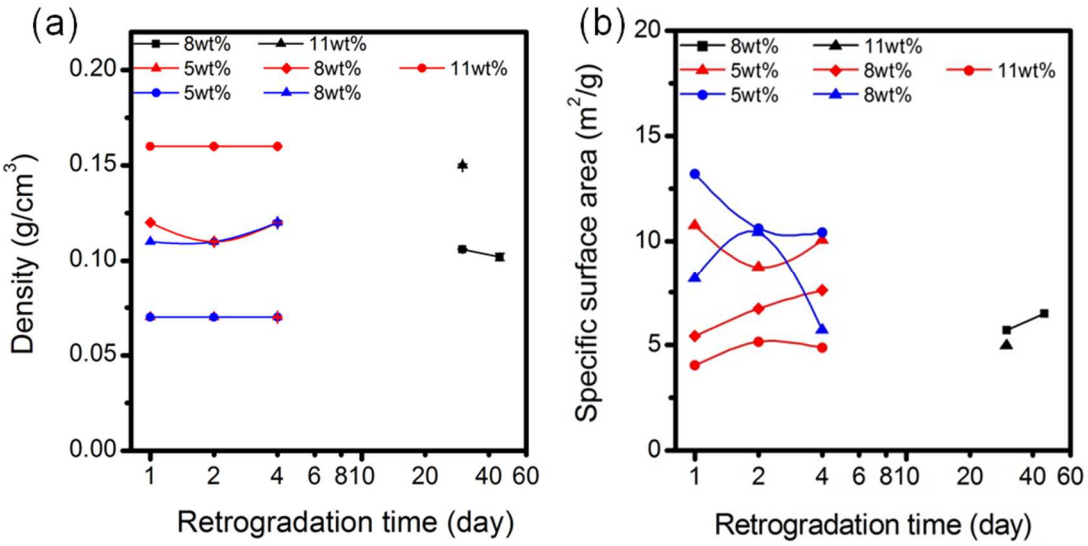


**Figure 7.** (a) Density and (b) specific surface area of cryogels from starch different concentrations and sources as a function of retrogradation time. Black, red, and blue data points correspond to waxy maize, potato, and pea starch cryogels, respectively. The lines are given to guide the eye. When standard deviations for density values are not seen, they are within the dimensions of the symbol.

The specific surface area of all cryogels (Figure 7b) is very low, within 3 - 13 $m^2/g$, which is at least 20-30 times lower than that of aerogels (see Figure 5b). We consider all values obtained for cryogels being similar within experimental errors which is around 10 $m^2/g$. Thus, no trend can be deduced.

## 4. Discussion

Based on all results obtained, we propose the following structure evolution in starch gels resulting in different aerogel morphology and properties. It is known that during retrogradation amylose associates into parallel double helices connected by amorphous regions, the whole forms semi-crystalline clusters (Putaux et al., 2000). We assume that at the early stages of retrogradation, amylose network with large pores, loose ends and junctions based of semi-crystalline clusters is formed (Figure 8); these gels are weak. At this stage, amylopectin starts to slowly associate to form necklace-like nano-structures (Putaux et al., 2000). With the increase of retrogradation time the crystallinity increases and gel becomes stronger: amylose chains, if present, form more and more junction zones leading to network reinforcement and ramification, the latter inducing the increase of specific surface area of aerogels. For the neat amylopectin solutions, it was shown that amylopectin forms a fractal network built of necklace-like structures (Putaux et al., 2000). We suppose that these nano-structures are too weak to resist solvent/non-solvent exchange: they collapse into much larger entities according to spinodal phase separation mechanism. We also hypothesize that with the increase of retrogradation time, amylose does not form longer and/or thicker “zip”-type structures which would lead to the decrease of specific surface area of aerogels. We assume that it is larger number of crystalline junctions that are formed with longer retrogradation resulting in stronger gels with higher crystallinity and more ramified network, the latter reflected by the increase of aerogels specific surface area (Figure 8). Higher amylose content in pea starch amplifies this phenomenon. It may also be possible that the presence of amylopectin in pea and potato starches prevents amylose condensing into thick aggregates, as was found for amylose alone in (Putaux et al., 2000), thus helping network ramification. As at higher amylose content gels are stronger, the shrinkage during aerogels' preparation is lower and the density of aerogels is also lower as compared to that of low-amylose content starch aerogels. The influence of amylose content of aerogel and cryogel density and on aerogel specific surface area is summarized in Figure 9.

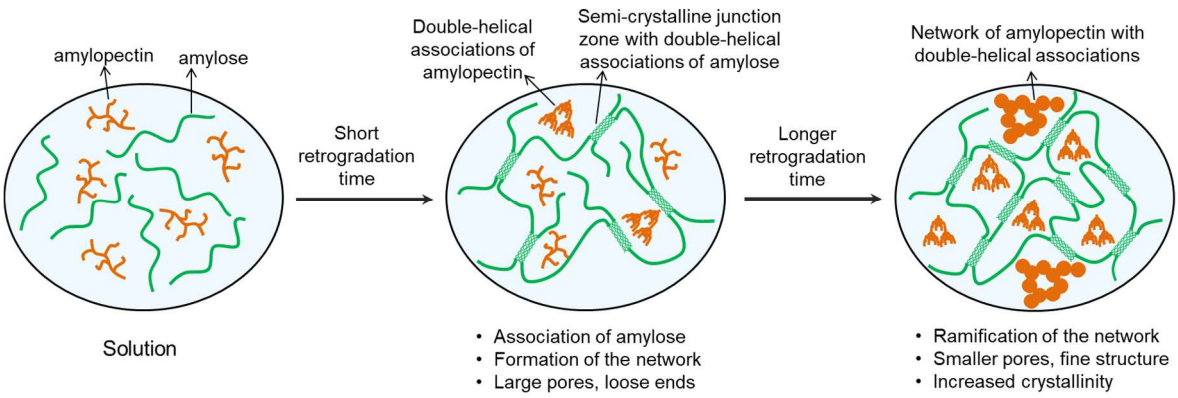


**Figure 8.** A schematic presentation of structure evolution in starch gels with the increase of retrogradation time.

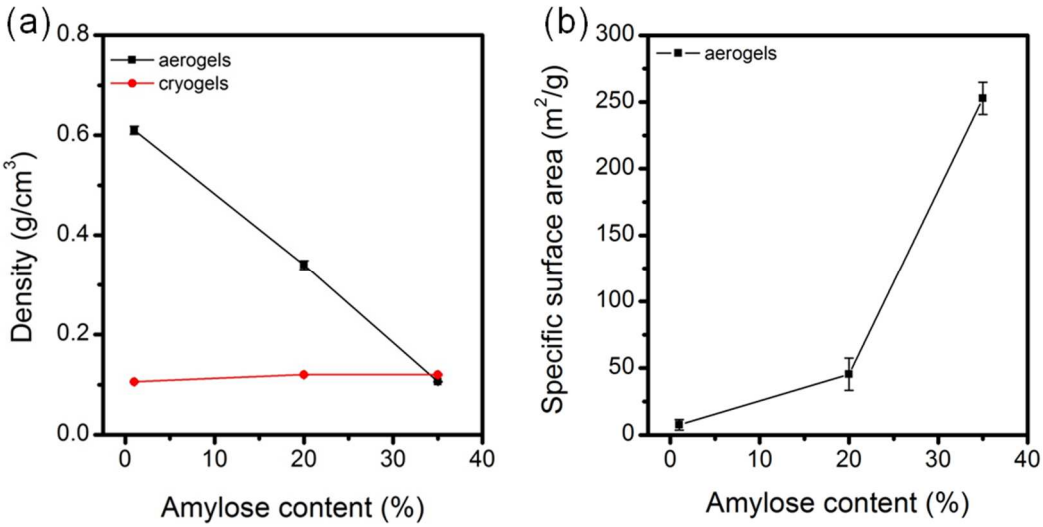


**Figure 9.** Density (a) and specific surface area (b) of starch aerogels and cryogels from 8 wt% solutions as a function of amylose content. The retrogradation time is 4 days for pea and potato starches and 15 days for waxy maize. The lines are given to guide the eye. When standard deviations values are not seen, they are within the dimensions of the symbol.

In the view of the said above, a schematic presentation summarizing structure evolution in all samples studied as a function of amylose content, starch concentration and retrogradation time is presented in Figure 10. In all the cases, with the increase of starch concentration and retrogradation time, the specific surface area of aerogels increases as the network becomes more ramified. Pea starch aerogels with the highest amylose content (33~36%) possess the highest specific surface area

due to the finest morphology amylose network (see Figure 9b). As pea starch gels are the strongest, their density is the lowest (Figure 9a). Potato aerogels with 18-21% of amylose present a mixed morphology of amylopectin beads and amylose network. Their specific surface area is lower than that of pea starch aerogels, and as the gels are weaker, the density is higher due to stronger shrinkage (Figure 9a). Waxy maize starch aerogels with only 1 % of amylose have the largest pores with the lowest specific surface area and the highest density (Figure 9).

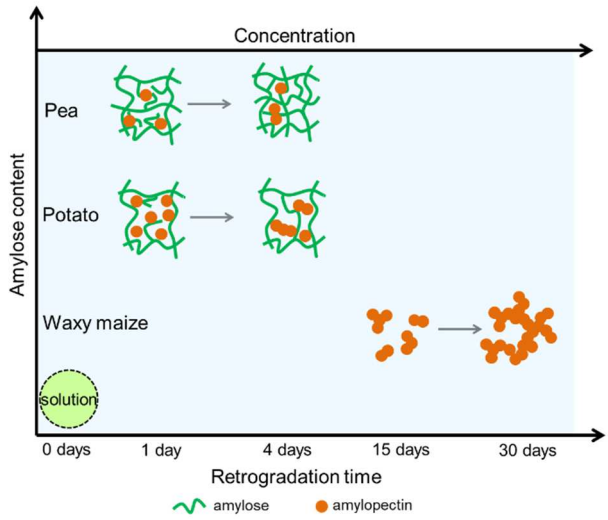


**Figure 10.** A schematic presentation summarizing structure evolutions in all starch samples, as deduced from aerogel morphology and properties, as a function of amylose content, starch concentration and retrogradation time. “0 days” correspond to the initial solution.

Various morphologies obtained in porous starches are interesting for different biomedical applications, in particular as no toxic compounds were used. For example, larger pores are suitable for making scaffolds for cells growth, and smaller pores are attractive for control release applications.

## 5. Conclusions

Highly porous starch materials were made from starch gels using two ways of drying: with supercritical $CO_2$ and freeze-drying. The influence of starch type (amylose content) and process parameters (starch concentration and retrogradation time) on the morphology, density and specific surface area were systematically studied and correlated with relative crystallinity and gel strength.

Drying mode had a significant impact on the properties of the dry material: freeze-dried starch gels had lower density and much lower specific surface area as compared to those of aerogels. This was

445 an expected result as the morphology and properties of materials freeze-dried from water are
446 dominated by the growth of ice crystals. Relative crystallinity dropped significantly after starch
447 dissolution-retrogradation-drying but was not influenced by the drying mode.

448 As drying with supercritical $CO_2$ is well preserving the morphology of starch gels, amylose content
449 and retrogradation time were playing an important role in the understanding of aerogel properties.
450 Higher amylose content, higher relative crystallinity and gel strength, lower sample shrinkage and
451 lower aerogel density. Different ways of amylose and amylopectin chains reorganization during
452 retrogradation and their different gelation kinetics is evidenced by the evolution of aerogel specific
453 surface area: pea starch aerogels possess the highest surface area, followed by potato and then by
454 waxy maize starch. With retrogradation, amylose forms more and more fine network leading to the
455 increase of aerogel surface area. At very long retrogradation times amylopectin (waxy maize starch) is
456 also gelling, but the gels are weak and shrinking during processing, resulting in higher density and
457 lower specific surface area.

458 The results obtained offer a new way of investigation of starch gels properties using drying with
459 supercritical $CO_2$. Opposite to freeze-dried starch, aerogels reflect the structure and its evolution in
460 starch gels; this mode of drying can thus be used as a tool for a deeper understanding of the structure
461 and properties of starch gels.

462

463 ## Acknowledgments

464 Authors are grateful to Roquette for sponsoring the work and providing starches, to Pierre Ilbizian
465 (PERSEE, MINES ParisTech) for the supercritical $CO_2$ drying, to Suzanne Jacomet (CEMEF, MINES
466 ParisTech) for the help with SEM and to Gabriel Monge (CEMEF, MINES ParisTech) for performing
467 XRD.

468

469

470

471

## References


Buchtová, N., & Budtova, T. (2016). Cellulose aero-, cryo- and xerogels: towards understanding of morphology control. *Cellulose,* 23, 2585-2595.

Buchtova, N., Pradille, C., Bouvard, J. L., & Budtova, T. (2019). Mechanical properties of cellulose aerogels and cryogels. *Soft Matter,* 15, 7901-7908.

Budtova, T. (2019). Cellulose II aerogels: a review. *Cellulose,* 26, 81-121.

Chau, M., De France, K. J., Kopera, B., Machado, V. R., Rosenfeldt, S., Reyes, L., et al. (2016). Composite Hydrogels with Tunable Anisotropic Morphologies and Mechanical Properties. *Chemistry of Materials,* 28, 3406-3415.

Cheetham W.H. N., & Tao, L. ( 1998). Variation in Crystalline Type with Amylose Content in Maize Starch Granules An X-Ray Powder Diffraction Study. *Carbohydrate Polymers,* 36, 277-284.

Druel, L., Bardl, R., Vorwerg, W., & Budtova, T. (2017). Starch Aerogels: A Member of the Family of Thermal Superinsulating Materials. *Biomacromolecules,* 18, 4232-4239.

García-González, C. A., & Smirnova, I. (2013). Use of supercritical fluid technology for the production of tailor-made aerogel particles for delivery systems. *The Journal of Supercritical Fluids,* 79, 152-158.

García-González, C. A., Uy, J. J., Alnaief, M., & Smirnova, I. (2012). Preparation of tailor-made starch-based aerogel microspheres by the emulsion-gelation method. *Carbohydrate Polymers,* 88, 1378-1386.

Glenn, G. M., & Irving, D. W. (1995)Starch-Based Microcellular Foams. *Cereal Chemistry,* 72, 155-161.

Glenn, G. M., Klamczynski, A., Chiou, B. S., Orts, W. J., Imam, S. H., & Wood, D. F. (2008). Temperature Related Structural Changes in Wheat and Corn Starch Granules and Their Effects on Gels and Dry Foam. *Starch - Stärke,* 60, 476-484.

Groult, S., & Budtova, T. (2018a). Thermal conductivity/structure correlations in thermal super-insulating pectin aerogels. *Carbohydrate Polymers,* 196, 73-81.

497 Groult, S., & Budtova, T. (2018b). Tuning structure and properties of pectin aerogels. *European*
498 *Polymer Journal,* 108, 250-261.
499 Hamedi, M., Karabulut, E., Marais, A., Herland, A., Nystrom, G., & Wagberg, L. (2013). Nanocellulose
500 aerogels functionalized by rapid layer-by-layer assembly for high charge storage and beyond.
501 *Angewandte Chemie. International Ed. In English,* 52, 12038-12042.
502 Himmel, B., Gerber, T., Biirger, H., Holzhfiter, G., & Olbertz, A. (1995). Structural characterization of
503 $SiO_2$-$A1_20_3$ aerogels. *Journal of Non-Crystalline Solids,* 186, 149-158.
504 Kistler, S. S. (1931). Coherent expanded aerogels and gellies. *Nature,* 127, 741.
505 Komiya, T., & Nara, S. (1986). Changes in Crystallinity and Gelatinization Phenomena of Potato Starch
506 by Acid Treatment. *Starch-Starke,* 38, 9-13.
507 Korhonen, O., & Budtova, T. (2020). All-cellulose composite aerogels and cryogels. *Composites Part A:*
508 *Applied Science and Manufacturing*, 137, 106027
509 Lavoine, N., & Bergström, L. (2017). Nanocellulose-based foams and aerogels: processing, properties,
510 and applications. *Journal of Materials Chemistry A,* 5, 16105-16117.
511 Ma, Z., Ma, M., Zhou, D., Li, X., & Hu, X. (2019). The retrogradation characteristics of pullulanase
512 debranched field pea starch: Effects of storage time and temperature. *International Journal*
513 *of Biological Macromolecules,* 134, 984-992.
514 Mallepally, R. R., Bernard, I., Marin, M. A., Ward, K. R., & McHugh, M. A. (2013). Superabsorbent
515 alginate aerogels. *The Journal of Supercritical Fluids,* 79, 202-208.
516 Mehling, T., Smirnova, I., Guenther, U., & Neubert, R. H. H. (2009). Polysaccharide-based aerogels as
517 drug carriers. *Journal of Non-Crystalline Solids,* 355, 2472-2479.
518 Nakamatsu, J., Torres, F. G., Troncoso, O. P., Min-Lin, Y., & Boccaccini, A. R. (2006). Processing and
519 Characterization of Porous Structures from Chitosan and Starch for Tissue Engineering
520 Scaffolds. *Biomacromolecules,* 7, 3345-3355.
521 Pierre A. C. (2011). History of aerogels. In M. A. Aegerter et al (Eds), Aerogels handbook, advances in
522 sol–gel derived materialsand technologies (pp. 813–831). Springer, New York

Pircher, N., Carbajal, L., Schimper, C., Bacher, M., Rennhofer, H., Nedelec, J. M., et al. (2016). Impact of selected solvent systems on the pore and solid structure of cellulose aerogels. *Cellulose (Lond),* 23, 1949-1966.

Putaux, J. L., Bule, A., & Chanzy, H. ( 2000,). Network Formation in Dilute Amylose and Amylopectin Studied by TEM. *Macromolecules,* 33, 6416-6422.

Robitzer, M., David, L., Rochas, C., Renzo, F. D., & Quignard, F. (2008). Nanostructure of Calcium Alginate Aerogels Obtained from Multistep Solvent Exchange Route. *Langmuir,* 24, 12547-12552.

Rooke, J., Passos, C. M., Chatenet, M., Sescousse, R., Budtova, T., Berthon-Fabry, S., et al. (2011). Synthesis and Properties of Platinum Nanocatalyst Supported on Cellulose-Based Carbon Aerogel for Applications in PEMFCs. *Journal of the Electrochemical Society,* 158, B779-B789.

Sai, H., Fu, R., Xing, L., Xiang, J., Li, Z., Li, F., et al. (2015). Surface modification of bacterial cellulose aerogels' web-like skeleton for oil/water separation. *ACS Appl Mater Interfaces,* 7, 7373-7381.

Saliger, R., Heinrich, T., Gleissner, T., & Fricke, J. (1995). Sintering behaviour of alumina-modified silica aerogels. *Journal of Non-Crystalline Solids,* 186, 113-117.

Sescousse, R., Gavillon, R., & Budtova, T. (2011). Aerocellulose from cellulose–ionic liquid solutions: Preparation, properties and comparison with cellulose–NaOH and cellulose–NMMO routes. *Carbohydrate Polymers,* 83, 1766-1774.

Shi, M., & Gao, Q. (2016). Recrystallization and in vitro digestibility of wrinkled pea starch gel by temperature cycling. *Food Hydrocolloids,* 61, 712-719.

Silva, E. K., Azevedo, V. M., Cunha, R. L., Hubinger, M. D., & Meireles, M. A. A. (2016). Ultrasound-assisted encapsulation of annatto seed oil: Whey protein isolate versus modified starch. *Food Hydrocolloids,* 56, 71-83.

Soest, J. J. G. V., Tournois, H., Wit, D. D., & Vliegenthart, J. F. G. (1995). Short-Range Structure in (Partially) Crystalline Potato Starch Determined with Attenuated Total Reflectance Fourier-Transform IR Spectroscopy. *Carbohydrate Research,* 279, 201-214.

549 Spada, J. C., Norena, C. P., Marczak, L. D., & Tessaro, I. C. (2012). Study on the stability of beta-
550 carotene microencapsulated with pinhao (Araucaria angustifolia seeds) starch. *Carbohydrate*
551 *Polymers,* 89, 1166-1173.
552 Svagan, A. J., Samir, M. A. S. A., & Berglund, L. A. (2008). Biomimetic Foams of High Mechanical
553 Performance Based on Nanostructured Cell Walls Reinforced by Native Cellulose Nanofibrils.
554 *Advanced Materials,* 20, 1263-1269.
555 Ubeyitogullari, A., & Ciftci, O. N. (2016). Formation of nanoporous aerogels from wheat starch.
556 *Carbohydrate Polymers,* 147, 125-132.
557 Ulker, Z., & Erkey, C. (2014). An emerging platform for drug delivery: aerogel based systems. *Journal*
558 *of Controlled Release,* 177, 51-63.
559 Zhang, B., Wang, K., Hasjim, J., Li, E., Flanagan, B. M., Gidley, M. J., et al. (2014). Freeze-drying
560 changes the structure and digestibility of B-polymorphic starches. *Journal of Agricultural and*
561 *Food Chemistry,* 62, 1482-1491.
562 Zhang, H., Hou, H., Liu, P., Wang, W., & Dong, H. (2019). Effects of acid hydrolysis on the
563 physicochemical properties of pea starch and its film forming capacity. *Food Hydrocolloids,*
564 87, 173-179.
565 Zhao, H. B., Chen, M., & Chen, H. B. (2017). Thermally Insulating and Flame-Retardant
566 Polyaniline/Pectin Aerogels. *ACS Sustainable Chemistry & Engineering,* 5, 7012-7019.
567 Zhu, F. (2019). Starch based aerogels: Production, properties and applications. *Trends in Food Science*
568 *& Technology,* 89, 1-10.
569 Zou, F., Peng, L., Fu, W., Zhang, J., & Li, Z. (2015). Flexible superhydrophobic polysiloxane aerogels for
570 oil–water separation via one-pot synthesis in supercritical CO2. *RSC Advances,* 5, 76346-
571 76351.
572 Zou, F., Yue, P., Zheng, X., Tang, D., Fu, W., & Li, Z. (2016). Robust and superhydrophobic
573 thiourethane bridged polysilsesquioxane aerogels as potential thermal insulation materials.
574 *Journal of Materials Chemistry A,* 4, 10801-10805.